American Mineralogist, Volume 87, pages 1077–1089, 2002

Analytical techniques for volatiles: A case study using intermediate (andesitic) glasses

P.L. KING,[1,*] T.W. VENNEMANN,[2] J.R. HOLLOWAY,[1,3] R.L. HERVIG,[1,4] J.B. LOWENSTERN,[5] AND J.F. FORNERIS[1]

[1]Geology Department, Arizona State University, Tempe, Arizona 85287, U.S.A.
[2]Institut Geochemie, Wilhelmstr. 56, D-72076, Tübingen, Germany
[3]Chemistry Department, Arizona State University, Tempe, Arizona 85287, U.S.A.
[4]Center for Solid State Science, Arizona State University, Tempe, Arizona 85287, U.S.A.
[5]U.S. Geological Survey, MS 910, 345 Middlefield Road, Menlo Park, California 94025, U.S.A.

ABSTRACT

Small-scale analyses of volatiles in minerals and glasses provide information on how volatiles influence high-temperature geologic processes and low-temperature alteration processes. Four techniques for determining the C-O-H volatile contents of andesitic glasses are compared: manometry, secondary ion mass spectrometry, micro-Fourier transform infrared spectroscopy, and a technique where the H_2O content is calculated using the difference between electron microprobe analysis totals and 100% sum. We present a method to determine the H content of a wide range of glass and mineral compositions using secondary ion mass spectrometry and a model for calibration factors. The extinction coefficients for H-O volatile contents in intermediate composition synthetic glasses are determined, and it is demonstrated that C-O speciation changes as total H_2O content increases, with molecular CO_2 decreasing, CO_3^{2-} increasing, and carbonate peak splitting increasing. For glasses with low H_2O content and oxy-substituted minerals, the methods of choice for volatile analysis are secondary ion mass spectrometry or micro-Fourier transform infrared spectroscopy.

INTRODUCTION

Volatile components, such as water and carbon dioxide, influence the chemical and physical properties of minerals and igneous melts and, hence, have a controlling effect on many high-temperature geologic processes, as well as low-temperature alteration processes and weathering. For instance, the H content of a mineral may relate to its crystallization conditions, and volatile exsolution from a melt can trigger volcanic eruptions or contribute to an ore-bearing magmatic vapor phase (e.g., reviews in Carroll and Holloway 1994). To understand these processes better, it is useful to analyze volatiles in minerals and glasses using micro-analytical techniques such as secondary ion mass spectrometry (SIMS, or ion microprobe), micro-Fourier transform infrared spectroscopy (micro-FTIR), or by calculating the difference of an electron probe micro-analysis total from 100 wt%. These techniques allow the analyst to choose an appropriate analysis area and may provide information on the zonation of volatiles and diffusion processes for volatiles.

SIMS analysis has the advantage of ease of sample preparation and small areas of analysis (<200 μm^2). However, calibrations are not straightforward because sample chemistry affects the yield of H ions (Delaney and Karsten 1981; Shimizu 1986; Steele 1986; Wilson et al. 1989; Ottolini et al. 1995; Hauri et al. 2002). Currently, H analysis of an unknown sample by SIMS relies on calibrations based on samples of similar and known composition. The curves are anchored by samples with a range of H content analyzed using bulk techniques, such as Karl-Fischer titration or manometry (Ihinger et al. 1994). Presently, the SIMS method suffers from the fact that appropriate calibrations are rare or non-existent. It would be useful if a model existed to determine the sensitivity of SIMS for measurements of H content in a wide range of mineral or glass compositions.

Micro-FTIR analysis has the advantage of detecting volatile speciation in samples; for example, OH^-, H_2O_{mol} (molecular H_2O), $CO_{2\,mol}$ (molecular CO_2), and CO_3^{2-}, all of which are found in natural glasses. Analyses of geologic samples are generally performed in transmission mode on areas of about 1500 to 8000 μm^2. Transmission micro-FTIR analysis provides ample signal for the detector, but has several disadvantages: mineral specimens must be oriented crystallographically, samples must be prepared as doubly polished wafers (especially difficult for glass inclusion work), and FTIR calibration factors, known as extinction coefficients, must be known. Extinction coefficients for volatile species are known for some glass compositions and these data have been incorporated in empirical models, for H-O species extinction coefficients (Dixon et al. 1995; Jakobsson 1997; Ohlhorst et al. 2001; Mandeville et al. 2002) and CO_3^{2-}

* Present address: Department of Earth Sciences, University of Western Ontario, London ON N6A 5B7 Canada. E-mail: plking@uwo.ca

extinction coefficients (Dixon and Pan 1995). Few calibration studies of glass wafers using micro-FTIR have systematically examined samples that contain mixed C-O-H species, despite the fact that most geologic samples contain mixed species. Also, there are few studies that use transmission micro-FTIR data to examine the behavior of C-O speciation in polished glass wafers as a function of H_2O content (Taylor 1990; Kohn and Brooker 1994; Jakobsson 1997).

Electron probe micro-analysis is a technique that is easily accessible for most Earth scientists, the sample preparation is routine, and small areas can be analyzed (for a 20 μm beam diameter the area is <320 μm^2). The deficit between an electron microprobe total and 100% has been used to calculate the H_2O content of andesitic to high-silica glasses (Devine et al. 1995) and minerals. Numerous authors have shown that this method is inaccurate for minerals with substantial Fe^{3+}/Fe^{2+} and oxy-substitution (e.g., Dyar et al. 1993; King et al. 1999). For glasses, care needs to be taken in an analysis to avoid Na-"loss" and Al- and Si-"grow in," and samples with less than 1 wt% H_2O content provide ambiguous results (Morgan and London 1996). Again, few studies have examined the accuracy and precision of electron probe micro-analysis using samples with mixed C-O-H species.

In this paper, we investigate methods for analyzing C-O-H volatiles via bulk manometry, SIMS, micro-FTIR, and calculation of volatile contents using the difference between electron microprobe analysis totals and 100% sum. We chose to study glasses to avoid crystallographic effects that complicate measurements. Andesite was chosen because few calibration factors have been determined for SIMS and micro-FTIR, even though andesitic composition glass occurs in tektites, melt inclusions, and matrix glass. Furthermore, andesitic compositions provide insight on C-O-H speciation in melts because andesites contain both CO_3^{2-} and $CO_{2\,mol}$ species, in contrast to rhyolites that only contain $CO_{2\,mol}$ and basalts that only contain CO_3^{2-} (review in Blank and Brooker 1994).

Experimental methods

For calibration purposes, it was necessary to synthesize glasses with high concentrations of total H_2O and total CO_2 (H_2O_{total} and $CO_{2\,total}$) at high pressure. We used natural andesite from Mt. Hood, Oregon, U.S.A, because it has a composition that is typical of calc-alkaline rocks (Table 1) and the melting conditions are known (Eggler and Burnham 1973).

Samples were enclosed in 5 mm diameter, Fe-doped Pt capsules designed to hold sufficient volumes for analysis (115 to 200 mg of sample) and minimize Fe diffusion from the sample to the capsule. Iron-doped Pt capsules were prepared in contact with molten Fe-rich trachyte in a one-atmosphere gas-mixing furnace, and then cleaned in HF. Volatile sources were added to obtain a range of H_2O and/or CO_2 contents for the purpose of calibration, thus some experiments were volatile undersaturated and others were volatile oversaturated. The volatile source was added to the capsule first, followed by the andesite powder (≤50 μm grain size). The volatile sources were distilled, deionized H_2O, and oxalic acid dihydrate ($H_2C_2O_4{\cdot}2H_2O$; OAD) or oxalic acid ($H_2C_2O_4$; OA), following Holloway et al. (1968). The capsule was arc-welded shut while wrapped in a frozen tissue to minimize volatile-loss. To test for leaks, capsules were submerged in hot mineral oil (>250 °C) for at least 20 s.

Experiments were performed in a 12.7 mm (0.5") non-end-loaded, piston-cylinder apparatus. The piston-cylinder furnace assemblies were made of NaCl-pyrex-Al_2O_3 pressure cells, NaCl and Al_2O_3 spacers, and an annealed graphite furnace; all were stored in a 100 °C oven prior to each experiment. To reduce C-diffusion from the furnace, finely powdered Al_2O_3 was packed between the capsule and the furnace using compressed air. Experiments with anomalous power consumption, indicating that the capsule touched the furnace, were discarded.

Temperature was measured with $W_{95}Re_5$-$W_{74}Re_{26}$ thermocouples and controlled to within 2 °C. The temperature gradient along a 6 mm vertical distance within the center of the furnace is less than 30 °C based on measurements of the thermal gradient with two thermocouples surrounded by alumina (King 1999). Pressure was measured with a Heise-gauge to within ± 4 MPa and no corrections were made for the pressure effect on the thermocouple e.m.f.

Experiments were initially over-pressurized by 10%, heated to 1300 °C (except one experiment to 1350 °C and one experiment at atmospheric pressure and 1150°), and the pressure was adjusted to 1.0 GPa once the run temperature was achieved (Table 2). Experiments lasted 2 h, except for four experiments that lasted only 20 min (Table 2). The samples were quenched approximately isobarically to below the glass transition temperature in about 4 seconds. Samples were not buffered for oxygen fugacity (f_{O_2}) because we wanted to maximize the sample size available for analysis, but it is likely close to the nickel-nickel oxide (NNO) buffer (King and Holloway 2002). Some H_2O-rich samples were discarded because they degassed over time and did not give reliable results.

Analytical methods

Manometry: H and C content and stable isotope compositions

The amounts of volatile H and C were determined at the University of Tübingen, following manometry techniques modified from Vennemann and O'Neil (1993). For volatile-saturated experiments, samples were crushed under reagent-grade acetone or ethanol and then hand picked under a binocular microscope to ensure that fluid-filled bubbles or quenched fluid phase solute were avoided. For volatile-undersaturated experiments, samples were crushed to 200–400 μm (following Newman et

Table 1. Starting compositions and average andesite composition

Oxides (wt%)	Mount Hood andesite* (MHA)	Mascota andesite† (MAS)
SiO_2	59.1	62.6
TiO_2	0.94	0.63
Al_2O_3	17.8	17.3
FeO	6.43	3.82
MnO	n.a.	0.19
MgO	3.05	0.44
CaO	6.85	0.86
Na_2O	4.27	9.80
K_2O	1.08	5.84
P_2O_5	n.a.	0.10
Total	99.5	98.8

* Eggler and Burnham (1973).
† Moore et al. (1995).

al. 1986) and weighed amounts were transferred into silica tubes. Each sample was covered with previously outgassed quartz grains and silica wool and then held at 10^{-6} mbar at room temperature for at least 12 h to remove surface H_2O. Samples were then heated to temperatures in excess of 1400 °C using an oxygen-propane torch until no further gas was released. Released volatiles were condensed in a liquid nitrogen trap (–196 °C). Non-condensable volatiles, including any reduced H or C species, were oxidized by CuO (at 700 °C). Water and CO_2 were subsequently separated using ethanol-liquid nitrogen slush traps (held at about –85 °C). The total CO_2 was then measured using a calibrated electronic manometer. The H_2O was transferred into a glass tube that was sealed with Zn and heated at 500 °C to produce H_2 for subsequent measurement using a Finnigan MAT 252 mass spectrometer. Weighed amounts of H_2O were always run in parallel with the samples to correct for daily variations in the tuning and sensitivity of the mass spectrometer.

For four samples, the volatiles were extracted separately at specific temperature increments: 200 °C for 2 h, 500 °C for 2 h, 750 °C for 2 h, and 1400 °C for 10 min (or until the pressures returned to background pressures for several minutes). During the 200, 500, and 750 °C steps, the volatiles were extracted using a small resistance furnace to heat the samples, with temperatures measured by a K-type thermocouple fixed next to the silica glass tube containing the sample.

The isotopic compositions [expressed in the typical δD and $\delta^{13}C$ values in per mil (‰) relative to VSMOW and VPDB, respectively] of volatiles released from select glasses were determined, in addition to H- and C-bearing components used in the experiments: distilled, deionized H_2O, OAD, an annealed piston-cylinder graphite furnace, and a used graphite furnace. The $^{13}C/^{12}C$ ratios of OAD and graphite were determined using an elemental analyzer on-line to a Finnigan MAT Delta plus XL mass spectrometer. For the $^{13}C/^{12}C$ measurements of OAD and graphite, the sample was placed in small Sn-foil holders, and combusted at temperatures in excess of 1100 °C using O_2, Cr_2O_3, and CoO. The D/H ratio of H_2O was analyzed as described previously (Vennemann and O'Neil 1993).

SIMS: H content

Hydrogen contents of andesite glasses were measured with a Cameca IMS-3F ion microprobe at Arizona State University (ASU) using techniques similar to King et al. (1999). The primary mass-filtered $^{16}O^-$ beam was accelerated to 12.5 kV at a current of 1 nA. The beam was initially rastered over a 25 × 25 μm^2 area for 7 min prior to analysis with a stationary beam (10 to 15 μm diameter). Positive secondary ions were accelerated to about 4.5 kV and those with 75 ± 20 eV excess kinetic energy were allowed to pass into the mass spectrometer (Ihinger et al. 1994). The instrument was operated at low mass resolution with the entrance and exit slits fully open.

Select samples of Mt. Hood andesite (MHA) and Mascota andesite (MAS) (Table 1) with H_2O_{total} wt% determined via manometry were used to determine calibration curves for the SIMS analyses (below). The hydrogen content of the remaining andesite samples was determined using the appropriate calibration curve. At least two determinations of $H^+/^{30}Si^+$ were made on each sample. Hydrogen background measurements were made periodically using nominally volatile-free samples: andesite and basanite glasses prepared in a 1-atm furnace and Lake County plagioclase (SM115900). Errors were calculated based on variations in the H background measurement for an entire analytical session.

Micro-FTIR: C-O-H speciation and concentrations

Micro-FTIR analyses were performed at the United States Geological Survey (USGS), Menlo Park, California. Spectra were collected using a Nicolet Magna 750 FTIR spectrometer with a KBr beam splitter, MCT-A detector, and a SpectraTech Analytical microscope. Each spectrum was obtained with 4 cm^{-1} resolution and 1000 to 1500 scans, with the background analyzed throughout a session. The entire system was continuously purged with dry air (containing about 5 ppm CO_2).

Glass for micro-FTIR analysis was taken from the central section of an experiment and mounted in orthodontic resin or Crystalbond at temperatures less than 80 °C to minimize sample degassing. The samples were doubly polished to a 1 μm finish, with thicknesses ranging from 50 to 320 μm (Table 3). Samples were cleaned in acetone and isopropyl alcohol and no residues from the mounting or cleaning medium were observed. A 100 μm diameter, doubly polished area was examined using an optical microscope to avoid bubbles and surface imperfections. Sample thicknesses were measured multiple times using a vertically mounted Mitutoyo micrometer at the USGS and errors are estimated at ±2 μm by comparison with measurements made using a similar micrometer at ASU.

FTIR absorption bands (Tables 3 and 4) were assigned following the studies summarized in Ihinger et al. (1994). We chose to determine extinction coefficients for the intermediate glasses and apply the Beer-Lambert law to determine concentrations, where: molar concentration = absorbance/(thickness × density × extinction coefficient). Another approach is to ratio a peak absorbance to a part of the FTIR spectrum that does not change, or is "spectrally isomorphic" (Agrinier and Jendrzejewsi 2000). We did not use the latter technique because a few of our samples were not spectrally isomorphic (see below).

To check sample homogeneity, two approaches were taken whenever possible. First, within a chip of a particular thickness, different locations were used for multiple analyses. Second, different chips of the same sample with different thicknesses were analyzed. To confirm that the Beer-Lambert law is valid (i.e., absorption is independent of thickness) seven samples were analyzed at a photographed location, thinned and then re-analyzed at the same location (Table 3).

Absorbance peaks were measured after curved baselines were subtracted. The baselines were fit in a precise, but not accurate, manner using French curves (similar to Zhang et al. 1997). For example, the 4500 cm^{-1} absorbance peaks were fitted by curves that were tangential to the minimum at about 4220 cm^{-1}, rather than by straight lines. We assessed reproducibility by fitting maximum and minimum baselines to the spectra and the variations from the tangential value are reported as error bars. The baseline under the 3550 cm^{-1} peak (O-H stretching = total H_2O) was assumed to be linear between 3800 and 2500 cm^{-1}, and since it is difficult to estimate an error on the

TABLE 2. Major element and bulk volatile compositions of andesite glasses used for calibrations

Sample	NVFA	Juli12	Juli9	MHA12	MHA18	MHA23	MHA25	MHA26	MHA27	MHA28
P(GPa), T(°C)	10^{-4}, 1150	1, 1300	1, 1300	1, 1300	1, 1300	1, 1300	1, 1300	1, 1350	1, 1300	1, 1300
Run duration (min)	720	120	120	120	120	120	120	120	120	120
Bubbles	v. few	yes	one large	few	yes	v. few	no	no	v. few	no
Excess volatiles	no	yes	yes	yes	yes	yes	no	no	no	no
No. probe analyses	6	7	7	5	5	5	7	8	5	7
wt%										
SiO_2	59.76	56.80	59.98	57.25	55.70	59.57	59.56	58.46	59.30	59.09
TiO_2	0.91	0.89	0.86	0.86	0.84	0.92	0.88	0.86	0.88	0.84
Al_2O_3	18.62	17.42	18.34	16.96	17.10	18.07	17.95	17.50	17.66	17.72
FeO_{TOT}	5.91	5.67	5.37	5.37	5.15	5.25	5.40	5.07	5.01	4.86
MnO	0.12	0.11	0.06	0.11	0.07	0.08	0.07	0.09	0.08	0.07
MgO	2.91	2.86	2.57	2.39	2.44	2.66	2.62	2.55	2.58	2.64
CaO	6.39	5.75	5.71	5.40	5.71	6.05	5.95	5.71	5.79	5.92
Na_2O	4.21	4.70	4.56	3.72	2.86	4.83	4.50	4.42	4.50	4.48
K_2O	0.85	0.91	0.91	0.82	0.80	0.93	0.90	0.89	0.90	0.90
P_2O_5	0.12	0.24	0.36	0.22	0.18	0.20	0.21	0.20	0.24	0.24
F	0.16	0.08	n.d.	n.d.	0.01	0.09	0.07	0.07	0.08	0.07
Total	99.96	95.44	98.73	93.09	90.92	98.65	98.11	95.82	97.02	96.83
Deficit (%, 1996–98) *	0.04	3.98	0.96	6.53	N/A	0.94	1.84	3.77	2.62	3.08
Deficit (%, 2001) *	N/A	N/A	1.14	2.87	9.08	N/A	N/A	3.41	1.32	N/A
Bulk volatiles †										
Manometry method		N/A	N/A	N/A	N/A	Bulk	Bulk	Bulk	Bulk	Bulk
H_2O% manometry (±0.1)		N/A	N/A	N/A	N/A	0.76	1.85	2.43	0.85	‡5.05
H_2O% SIMS		3.39 (0.35)	0 (0.30)	1.34 (0.82)	6.09 (0.17)	Calib.	Calib.	Calib.	Calib.	2.58 (1.35)
CO_2% added §	0.0	7.03 (XS)	3.23 (XS)	5.53 (XS)	0.03	0.73	0.03	0.63	0.43	0.03
CO_2% manom. raw (±0.05)	N/A	N/A	N/A	N/A	N/A	0.70	0.22	0.97	0.86	‡0.97
CO_2% manom. corr. ll	N/A	N/A	N/A	N/A	N/A	0.65	0.17	0.92	0.81	‡0.92

Notes: N/A = not analyzed or not applicable; n.d. = not detected.

* Deficit (%) = 100 - electron microprobe total - CO_2 content (by FTIR). Deficits are calculated based on measurements during either 1996–1998 or 2001.

† Manometry method refers to either heating the sample at one temperature (Bulk) or incrementally heating the sample (Incr.). Calib. refers to runs that were used for calibrating SIMS.

‡ This manometry data was excluded from the calibrations because it was in excess of our expectation for both H_2O and CO_2 (possible contamination). Furthermore, the manometry data did not agree with SIMS and FTIR analyses.

§ The initial concentration of CO_2 in Mt. Hood andesite starting material is less than 0.03 wt% (P. Middlestead, pers. com.). Therefore, the initial CO_2 content was calculated based on the amount of OAD added + 0.03 wt%. XS = excess fluid added.

ll CO_2% manom. corr. is the CO_2 wt% determined by manometry is corrected by subtracting the blank value (0.05%) or, for incrementally-heated samples, by subtracting the CO_2 content released at 200 °C and subtracting the blank value.

linear baseline we assume a 10% error on the 3550 cm^{-1} peak absorbance measurement. Absorbance peaks for the 3500 cm^{-1} peak with greater than 1.5 absorbance units were not used (following Newman et al. 1986).

It was difficult to draw a baseline under the CO_3^{2-} doublets (about 1550 and 1420 cm^{-1}) because the spectra are not isomorphic due to two strong underlying bands: the ~1300 cm^{-1} aluminosilicate band and the 1630 cm^{-1} H_2O_{mol} band (Fig. 1). To improve CO_3^{2-} doublet baseline precision, spectra were printed at similar scales and the same portion of a French curve was used for baselines (Figs. 1a and 1c). We decided to use this technique because it is reproducible, results in peaks that are close to gaussian in shape, and can be used for other glass compositions. In an effort to evaluate the error associated with this technique three French curve baselines were fit (i, ii, and iii in Fig. 1c), with the middle baseline (fit ii in Fig. 1c) used and the maximum error reported. A second approach is to use a baseline spectra from a nominally volatile-free andesite (NVFA), but because the ~1300 cm^{-1} band has a slope that varies dependent on the composition of the glass there is uncertainty in where to locate the baseline (Fig. 1c). Furthermore, the French curve baseline method (ii) is generally within error of the NVFA baseline method (Fig. 1c). We investigated the possibility of fitting the H_2O_{mol} peak at ~1630 cm^{-1} using spectra from a H-rich, C-poor andesite as a baseline (e.g., MHA18; Fig. 1c), but found poor fits in the 1800 cm^{-1} region, presumably due to modification in the aluminosilicate structure. We also tried subtracting spectra from H-poor, C-bearing andesites (e.g., Juli9; Fig. 1c) but because the CO_3^{2-} peaks shift position with H content (e.g., Jakobsson 1997; King and Holloway 2002; Figure 1c) that method was not satisfactory. Another useful method is to prepare a synthetic baseline by combining (1) a baseline of NVFA; (2) a baseline based on a H-rich, C-poor andesite for the H_2O_{mol} peak at ~1630 cm^{-1}; and (3) a straight line to account for the changing slope of the 1300 cm^{-1} aluminosilicate band (following S. Newman, personal communication, 1998) similar to Macpherson et al. 1999). However, that technique requires prior knowledge of the nominally volatile-free andesite baseline and an H-rich, C-poor andesite spectra, both of which may be difficult to prepare for samples such as melt inclusions. In sum, we found that the French curve baseline method was within error of other approaches and the French curve technique is advantageous when determining the volatile contents of samples with unknown volatile-free or C-free baselines.

Glass densities were calculated in two ways and the average value used (Table 3). The first method used specific refractive energy and refractive index data and assumed that all Fe is Fe^{2+}

TABLE 2.—*extended*

MHA30	MHA31	MHA41	MHA44	MHA6
1, 1300	1, 1300	1, 1300	1, 1300	1, 1300
20	20	20	20	120
no	no	v. few	v. few	one large
no	no	no	little	yes
5	5	6	6	10
wt%				
58.96	59.25	58.36	58.10	58.79
0.85	0.86	0.84	0.85	0.85
18.36	18.48	18.16	18.35	17.31
5.39	5.62	5.47	5.36	5.40
0.06	0.11	0.10	0.09	0.09
2.65	2.7	2.57	2.59	2.54
5.96	6.04	5.92	5.80	5.70
4.51	4.57	4.40	4.34	4.23
0.89	0.91	0.88	0.86	0.90
0.21	0.19	0.12	0.24	0.28
0.12	0.11	0.10	n.d.	n.d.
97.96	98.84	96.92	96.58	96.09
1.96	1.09	2.74	2.92	3.48
N/A	N/A	N/A	N/A	N/A
Bulk volatiles †				
Incr.	Incr.	Incr.	Incr.	N/A
2.48	1.09	2.69	3.7	N/A
2.31	1.16	3.06	3.34	2.62
(0.10)	(0.06)	(0.06)	(0.37)	(0.19)
0.03	0.03	0.23	0.73	7.23 (XS)
0.28	0.28	0.49	0.64	N/A
0.14	0.20	0.40	0.53	N/A

(Silver 1988). The second method is intended for silicate melts (Lange and Carmichael 1987), and we assumed that f_{O_2} was at NNO (King and Holloway 2002), and that the density of the glass is less than the melt by 15 g/L per wt% H_2O_{total} (e.g., Carroll and Blank 1997). In both calculations the effect of $CO_{2\,total}$ on density was ignored since the CO_2 concentrations are low and it is unlikely to have much effect on density, by analogy with the relatively small effect of CO_2 on viscosity for similar silicate compositions (Brearley and Montana 1989).

Electron probe micro-analysis: major element content

Each sample was cut lengthwise, mounted in Araldite epoxy or orthodontic resin, and polished to a 1 μm finish. Electron probe data were obtained at ASU using a JEOL JXA 8600 electron probe with wavelength dispersive spectroscopy and ZAF corrections. The calibration was checked using two hydrous MAS andesite glasses samples that were characterized by wet chemistry (Moore et al. 1995), and also a basanite (characterized by Oskarsson et al. 1982) that was melted in a one-atmosphere gas-mixing furnace so that it was nominally anhydrous. To assess electron beam damage and alkali element "loss" and Al- and Si-"grow in," glasses were analyzed under two conditions (King and Holloway 2002), with preference for a 15 kV, 10 nA, and a 15 to 20 μm beam, with Na and K analyzed first for 30 s each.

RESULTS

Sample characterization

Experimental products were clear, brown glasses with no visible surface coatings. Most runs were volatile undersaturated with respect to C and H and, accordingly, few or no bubbles were observed in most samples (Table 2). The volatile undersaturated samples with the least water (MHA23 and MHA27; Table 2) contained a few bubbles. The two volatile undersaturated experiments with the shortest run duration (20 min) contained a few (<1 vol%) tiny bubbles (MHA41 and MHA44). The presence of tiny bubbles in those experiments suggests that longer run times are preferable, even though other short experiments on melts with similar viscosities have produced adequate volatile-bearing glasses (Mysen 1976; Jakobsson 1997). Samples that were volatile supersaturated contained bubbles or, in a few cases, a fluid phase solute precipitate that approximates a volatile-rich rhyolite composition.

Multiple electron probe micro-analyses of the glasses did not reveal any heterogeneity beyond the analytical precision. The products were crystal-free based on petrographic and back-scattered electron imaging. In addition, a $^{12}C^-$ image over a 20 to 40 μm diameter area did not indicate any heterogeneity (E. Hauri, personal communication 1998). Despite using Fe-doped capsules, FeO was depleted up to 0.9 wt% (absolute), it is not expected that this small variation in FeO affects our calibration curves for the volatiles. Although it was not necessary for these synthesis (calibration) experiments to obtain equilibrium, an approach to equilibrium is suggested because two runs with similar H_2O_{total} contents yielded similar $CO_{2\,total}$, $CO_{2\,mol}$, and CO_3^{2-} contents (Table 3), even though one was oversaturated in C by a large amount (MHA23, Table 2) and the other only slightly oversaturated in C (MHA27, Table 2).

Manometric total H and C contents

The results of measurements of the total H and C contents by manometry, reported as H_2O_{total} and $CO_{2\,total}$ concentrations, are given in Table 2. Errors were evaluated based on the volume measurements. One sample (MHA28) had manometric H_2O and CO_2 contents that were higher than expected based on the amount added, SIMS and FTIR measurements; therefore, it is likely that the manometry values for this sample included contamination.

Manometric total H and C may include surface adsorbed, vesicle, and glass volatiles. We assumed that the contribution from fluid inclusions (bubbles) was negligible in our manometry samples because they were (1) mostly volatile-undersaturated (Table 2); (2) ground to 200–400 microns; and (3) we optically inspected the samples for bubbles prior to analysis. Thus, our discussion focuses on the surface adsorbed and glass volatiles.

The temperature at which the different volatile components are released is related to the composition of the glass, grainsize and geometry (e.g., Des Marais and Moore 1984; Des Marais 1986; Newman et al. 1986). To determine the contributions from the different fractions some workers have inferred specific temperature "cut-offs." For example, volatiles released from basaltic glasses at temperatures less than about 600 °C in large chips of basaltic glass (1–3 mm) have been ascribed to contamination (e.g., Macpherson et al. 1999), although in more felsic and/or water-rich compositions (of varying grainsize) water may be derived from the glass at temperatures below 200 °C (e.g., Newman et al. 1986; Zhang et al. 1991; Moore et al. 1998). This difference in volatile-release behavior is due to

TABLE 3. C-O-H speciation of andesite glasses used for calibrations

Sample	NVFA	Juli12	Juli9	MHA12	MHA18	MHA23	MHA25	MHA26	MHA27	MHA28
Bulk volatiles										
CO_2% manom. corr.	N/A	N/A	N/A	N/A	N/A	0.65	0.17	0.92	0.81	N/A
H_2O% used for FTIR calibration *	N/A	3.39 (0.35)	0 (0.30)	1.34 (0.82)	6.09 (0.17)	0.76 (0.10)	1.85 (0.10)	2.43 (0.10)	0.85 (0.10)	2.58 (1.35)
FTIR data †										
H_2O_{mol} %	0.0	2.20 (0.28)	n.d.	n.d.	4.14 (0.06)	n.d.	0.34 (0.04)	0.72 (0.07)	n.d.	1.90 (0.08)
OH^- %	0.0	1.32 (0.11)	0.14 (0.08)	1.08 (0.23)	1.41 (0.07)	0.31 (0.02)	0.86 (0.12)	1.12 (0.10)	0.30 (0.02)	1.59 (0.08)
H_2O_{total} %	0.0	3.52	n.d.	n.d.	5.55	n.d.	1.20	1.84	n.d.	3.49
$CO_{2\ mol}$ %	0.0	0.009 (0.001)	0.069 (0.011)	0.056 (0.013)	n.d.	0.077 (0.012)	0.006 (0.001)	0.033 (0.005)	0.077 (0.012)	0.004 (0.001)
CO_3^{2-} %	0.0	0.575 (0.058)	0.237 (0.029)	0.326 (0.062)	n.d. (0.034)	0.337 (0.005)	0.043 (0.037)	0.373 (0.028)	0.283 (0.016)	0.086 (0.008)
$CO_{2\ total}$ %		0.58	0.31	0.38	n.d.	0.41	0.05	0.41	0.36	0.09
Max. (Ave) CO_3^{2-} peak split-cm^{-1} (±4 cm^{-1})	N/A	90 (89)	120 (98)	103 (99)	n.d.	112 (109)	99 (97)	98 (94)	114 (108)	102 (94)
Density (g/L) ‡	2566 ± 43	2522 ± 1	2542 ± 43	2581 ± 31	2446 ± 43	2538 ± 49	2524 ± 35	2539 ± 3	2547 ± 20	2482 ± 14
FTIR Chip 1 Date	8.96	12.96	12.96	8.96	8.96	12.96	12.96	12.96	12.96	12.96
Analysis prefix	vfree3	xJ12	J9	12	18	x23	xx25	x26	x27	x28
Thickness (micrometers)	318	61	145	98	92	144	90	121	162	139
No. of analyses	1	2	3	3	2	2	2	2	2	3, §
FTIR Chip 2 Date	8.96	12.96	9.98		8.96	9.98	5.98	9.98	12.96	9.98,
Analysis prefix	vf1	xJ12	sj9		18	s23	mha25pk	s26	x27.2	t28
Thickness (micrometers)	65	54	140		105	150	99	120	170	54
No. of analyses	1	1	1		1	1, §	3	2, §	1	2, §
FTIR Chip 3 Date	12.96					9.98	9.98	9.98		
Analysis prefix	xvfree					s9823A	s25	t26		
Thickness (micrometers)	100					110	100	60		
No. of analyses	2					2,§	1	2, §		
FTIR Chip 4 Date	9.98									
Analysis prefix	vfa1									
Thickness (micrometers)	100									
No. of analyses	1									

* The error on the SIMS and manometry data was estimated based on the larger value of (1) the difference between the SIMS and manometry analyses, (2) the background variation for SIMS analyses, (c) volume measurements for manometry analyses.
† FTIR H-O species errors were calculated based on errors in the background subtraction of the absorbance measurements. FTIR CO- species errors were calculated using the largest error on either the background subtraction of the absorbance measurement or the error on the extinction coefficient.
‡ Density calculation averages two methods. Larger density value calculated following Lange and Carmichael (1987) with Fe_2O_3/FeO values calculated at NNO and a correction for H_2O% (Carroll and Blank 1997). The smaller density value was calculated following Silver (1988), assuming all Fe is FeO.
§ The same location was analyzed at two different thicknesses.

differences in the glass transition temperature, which depends on glass composition, including volatile content (e.g., Dingwell and Webb 1990).

We used incremental heating profiles to infer the contribution of volatiles dissolved in the glass (the desired quantity) and surface adsorbed volatiles (contamination). We decided to infer maximum glass transition temperatures for the glasses; based on the temperature at which substantial H_2O was released (Fig. 2; more than 0.10 wt%). For samples with 2 to 4 wt% H_2O_{total} content the inferred maximum glass transition temperature is about 500 °C, and for the sample with about 1 wt% H_2O_{total} content, the inferred maximum glass transition is below 725 °C (Fig. 2). This rationale leads to the assumption that volatile content measured below the inferred maximum glass transition temperature results from surface absorption. For the incrementally heated samples, surface adsorbed H_2O is very low (0.10 wt%) and $CO_{2\ total}$ contents are about 0.09 wt%, within error of the blank correction (0.05 wt% ± 0.05 wt%).

The $CO_{2\ total}$ contents of the glasses are difficult to measure because CO_2 is readily released from the glass and $CO_{2\ total}$ concentrations are low relative to the manometry error (±0.05 wt%). Another difficulty in measuring CO_2 is that carbon compounds (e.g., hydrocarbons) readily adsorb to glass and could contaminate the sample. This could be a particular problem for analytical methods where samples are analyzed at a single high temperature (e.g., combustion analyses). To minimize these problems in the samples that were measured at one high temperature a blank correction (0.05 wt% $CO_{2\ total}$) was subtracted to account for contamination (CO_2 percent manometry corrected values in Tables 2 and 3). For samples that were incrementally heated we subtracted the blank correction as well as the amount of CO_2 released at 200 °C that is likely to be surface adsorbed (Table 2).

Despite correcting for the blank, the corrected $CO_{2\ total}$ contents from manometry exceed the quantity initially added for most samples (Table 2). Samples that had only the natural CO_2

TABLE 3. — *extended*

MHA30	MHA31	MHA41	MHA44	MHA6
0.14	0.20	0.40	0.53	N/A
2.31	1.16	3.06	3.34	2.62
(0.17)	(0.06)	(0.40)	(0.63)	(0.19)
1.06	0.35	1.30	1.97	1.57
(0.08)	(0.03)	(0.06)	(0.18)	(0.12)
1.26	0.88	1.29	1.47	1.38
(0.08)	(0.06)	(0.11)	(0.07)	(0.05)
2.32	1.23	2.59	3.44	2.95
0.004	0.009	0.014	0.014	0.029
(0.001)	(0.001)	(0.002)	(0.002)	(0.005)
0.076	0.061	0.323	0.483	0.398
(0.011)	(0.032)	(0.048)	(0.040)	
0.08	0.07	0.34	0.50	0.43
99 (95)	105 (103)	92 (91)	91 (91)	97 (97)
2518 ± 31	2533 ± 45	2527 ± 21	2517 ± 13	2511 ± 6
5.98	5.98	5.98	5.98	8.96
mha30	mha31a	mha41c	mha44a	6.1
174	238	167	319	159
2	2	1	2	2
9.98	5.98	9.98	5.98	8.96
S30A	mha31c	mha41a	mha44b	6
180	221	97	155	218
1, §	2	2	2	1
9.98	9.98	9.98	9.98	
T30A	S31	S41A	S44A	
90	240	100	320	
2, §	1, §	1, §	1, §	
	9.98	9.98	9.98	
	T31A	T41A	T44A	
	60	40	50	
	2, §	2, §	2, §	

content of the starting material (CO_2 content < 0.03 wt%) have corrected manometry $CO_{2\ total}$ contents greater than or equal to 0.14 wt% (Table 2). The excess corrected $CO_{2\ total}$ content could have three sources: C from fluid-filled bubbles, C contamination during sample handling and measurement, or C diffusion into the melt from the graphite furnace during an experiment. Carbon contamination or fluid inclusion sources (assumed negligible; above) are unlikely to be the single source of excess CO_2 because micro-FTIR analyses indicate that C-O species are present in glasses that did not have CO_2 added. Contamination in the form of CO_2 dissolved in the distilled, deionized H_2O is likely insignificant because CO_2 solubility is low at room conditions, and the amount of H_2O added was typically less than 10 μL.

To evaluate whether the excess corrected $CO_{2\ total}$ could originate from carbon from the graphite furnace entering the capsule, carbon isotopes were measured on the four incrementally heated samples. Carbon isotope fractionation is likely to be negligible during the experiments because of the relatively high temperatures (1300 °C), relatively short reaction periods, and absence of a free fluid phase (except for MHA44). The findings of Brooker et al. (1998), who used the same apparatus, confirm our assumption. The weighted $\delta^{13}C$ values of the C released incrementally above 200 °C from the glasses are consistent with C-derivation from an organic source, such as the graphite furnace. For example, samples without added OAD (MHA30 $\delta^{13}C = -27.34‰$, MHA31 $\delta^{13}C = -25.73‰$) have values that are similar to annealed and unannealed furnaces ($\delta^{13}C = -25.9 \pm 0.1‰$). Although the isotopic data alone do not rule out an additional organic C source in the starting material, these data, combined with the FTIR observations (below), point to a contribution of C from graphite. In contrast, the experiments where OAD was added have $\delta^{13}C$ values of the C released incrementally above 200 °C close to the OAD value (MHA41 = –28.13‰, MHA44 = –28.71‰ and OAD = –28.57 ± 0.03‰). Those experiments probably had negligible C diffuse into the capsule because the C-gradient was relatively unfavorable (although the isotopic values cannot resolve that). To avoid introducing small amounts of C into C-deficient experiments, other techniques, such as surrounding the sample with a buffer capsule or Al_2O_3 tubing (Brooker et al. 1998), might be appropriate.

SIMS H contents

A SIMS calibration line for H_2O contents using an $^{16}O^-$ primary beam is shown in Figure 3 for the two andesites. The MHA samples define a calibration line with a slope of 0.24. The MAS samples define a calibration line with a slope of 0.25. The SIMS calibration line was used to determine the H content of samples not analyzed by manometry (Table 2) and to verify that the different locations in a sample showed little variation in H within error.

Micro-FTIR analyses: C-O-H speciation

FTIR spectroscopy indicates that the major volatile species in andesite are $CO_{2\ mol}$, H_2O_{mol}, OH^- and CO_3^{2-} (Table 3). A representative spectrum is shown in Figure 1.

We did not observe any reduced C species in the glasses: molecular CO peaks were not observed (^{12}CO band at 2185 cm^{-1}) and graphite was not observed optically or with SIMS images. Furthermore, no reduced species were observed in either fluid-filled bubbles or glasses using Raman spectroscopy (King 1999). This is in contrast to experiments at higher temperatures and pressures where C-diffusion into the capsule is greatly enhanced and reduced C-O species were observed in intermediate glasses (Brooker et al. 1998; Brooker et al. 1999).

The $CO_{2\ mol}$ peaks (~2350 cm^{-1}) most likely represent dissolved CO_2 in the glass, rather than CO_2 in bubbles, because bubbles are absent in most of the volatile undersaturated runs (Table 2), $CO_{2\ mol}$ concentrations are essentially constant within a sample, and peaks associated with bubbles (Stolper et al. 1987) are absent.

H-O species. As indicated above, several models exist for micro-FTIR extinction coefficients for H-O species in glasses (Dixon et al. 1995; Jakobsson 1997; Ohlhorst et al. 2001; Mandeville et al. 2002). Our results agree well with these models and other literature results (Table 4).

For H-O species, we assume that $C_{H_2O} = C_{5200} + C_{4500}$, where C_{H_2O} is the concentration of H_2O_{total} (wt%, measured using manometry or SIMS), C_{5200} and C_{4500} are the concentrations of H_2O_{mol} and OH^- respectively, $C_{5200} = (18.015\ A_{5200})/(d\ \varepsilon_{5200}\ \rho)$ and $C_{4500} = (18.015\ A_{4500})/(d\ \varepsilon_{4500}\ \rho)$, where 18.015 is the molecular weight (g/mol) of H_2O, A_{5200} and A_{4500} are the linear absorbances of the 5200 cm^{-1} and 4500 cm^{-1} bands respectively,

TABLE 4. FTIR bands, species and extinction coefficients.

Wavenumber 4 cm^{-1} resolution {Average}	Species	Vibration mode	Literature extinction coefficient ($L/mol/cm^{-1}$)	Extinction coefficient, this study ($L/mol/cm^{-1}$)
5200 {5209}	H_2O_{mol}	O-H stretch H-O-H bend	1.3 (calculation, Dixon et al. 1995) 1.10 +0.12/ –0.10 (phonolite, Carroll and Blank 1997) 1.6 ± 0.3 (dacite, Yamashita et al. 1997) 1.09 ± 0.04 (andesite, Mandeville et al. 2002) 1.34 ± 0.06 (Fe-Free andesite, Mandeville et al. 2002) 1.01/0.96 (andesite GG/GGpar, Ohlhorst et al. 2001) 1.06 (calculation, Ohlhorst et al. 2001)	1.08 ± 0.11
4500 {4503}	OH^-	Si-OH Al-OH	0.93 (calculation, Dixon et al. 1995) 1.25 +0.33/ –0.22 (phonolite, Carroll and Blank 1997) 0.94 ± 0.06 (dacite, Yamashita et al. 1997) 0.78 ± 0.04 (andesite, Mandeville et al. 2002) 1.14 ± 0.06 (Fe-Free andesite, Mandeville et al. 2002) 0.82/0.85 (andesite-GG/GGpar, Ohlhorst et al. 2001) 0.94 (calculation, Ohlhorst et al. 2001)	1.15 ± 0.17
3550 {3534}	H_2O_{total}	H-O-H symmetric stretch	61.43 ± 0.53 (andesite, Mandeville et al. 2002) 70.16 ± 0.79 (Fe-Free andesite, Mandeville et al. 2002) 68 ± 1 (dacite, Yamashita et al. 1997) 52–73 (glasses with 55–65 wt% SiO_2; Pandya et al. 1992)	70.3 ± 6.9
3100	shoulder of 3550 cm^{-1} peak			26.7 ± 6.2
1630 {1633}	H_2O_{mol}	H-O-H bend	42.28 ± 1.85 (andesite, Mandeville et al. 2002) 47.57 ± 1.98 (Fe-Free andesite, Mandeville et al. 2002) 42.7 (icelandite, Jakobsson 1997)	40.8 ± 4.1
2350 {2349}	$^{12}CO_{2\ mol}$	^{12}C-O asymmetric stretch	945 (Na-Al-Si glass, Fine and Stolper 1985) 1066 (rhyolite, Blank 1993) 796 ± 250 (haplo-phonolite synthesized at 1300°, Morizet et al. 2002) 890 (average, Morizet et al. 2002)	945 used
1500–1700 {1522}	CO_3^{2-}	O-C-O asymmetric stretch	271 (calculation, Dixon and Pan 1995)	271 used
1430–1350 {1422}	CO_3^{2-}	O-C-O asymmetric stretch	269 (calculation, Dixon and Pan 1995)	269 used

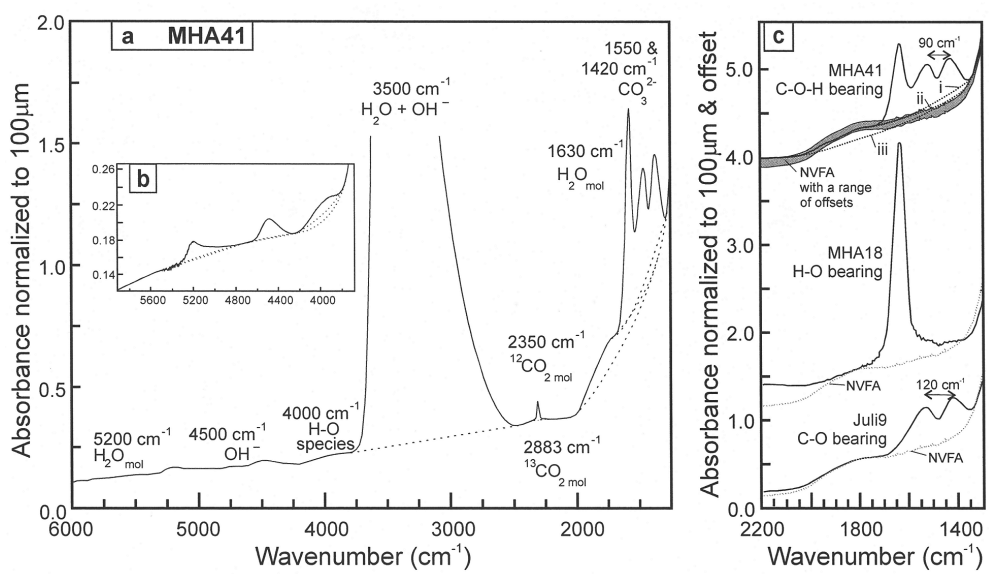

FIGURE 1. (**a**) Representative FTIR spectrum for a sample showing all C-O-H species (sample MHA41.97). The peaks corresponding to C-O-H absorbances are labeled and representative baseline curves shown. Peak height measurements were taken using the intermediate fitting baseline curve and errors were assigned based on the extreme baseline curves. (**b**) Expanded view of the 5200 and 4500 cm^{-1} peaks and the baseline curves. (**c**) Representative FTIR spectra showing the difficulties in fitting the H_2O_{mol} and CO_3^{2-} peaks. The spectra have been offset an arbitrary amount for clarity of comparison. The top spectrum (MHA41) shows the French curve fits (i, ii, and iii) and the nominally volatile-free andesite (NVFA) with a range of vertical offsets. The MHA18 spectrum is for an H-O bearing sample—the noise associated with the peak likely is due to the strong absorbance signal. The NVFA sample does not form a good baseline for this sample. The bottom spectrum is for a C-O bearing sample (Juli9). Note that the carbonate peak splitting is larger for this sample than for MHA41, which also contains H-O species. Some spectral resolution has been lost in the process of preparing this figure.

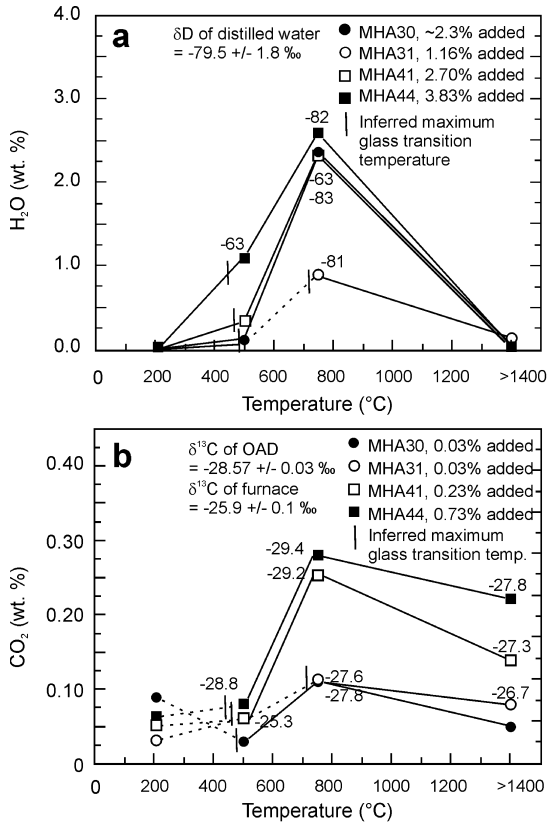

FIGURE 2. Plots of (**a**) H_2O and (**b**) CO_2 concentrations measured manometrically and extracted at different temperatures (200, 500, 750 and >1400X °C) for four samples (MHA30, MHA31, MHA41 and MHA44). Also given are the δD values (‰) of the extracted water and the $\delta^{13}C$ values (‰) of the extracted CO_2. Both diagrams show the inferred maximum glass transition temperature and dotted lines connect the volatile contents measured below that temperature.

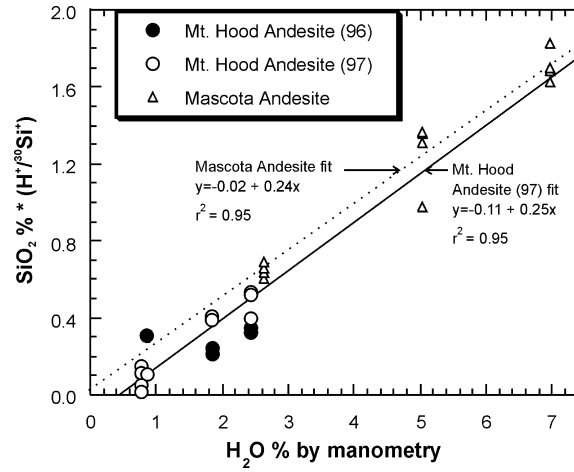

FIGURE 3. SIMS H calibration curves for the Mt. Hood andesite (MHA) (from Eggler and Burnham 1973) and Mascota andesite (MAS) (from Moore et al. 1995). SiO_2 wt% · $H^+/^{30}Si^+$ from SIMS analysis vs. H_2O_{total} wt% from manometry. Errors are evaluated based on variations in the H background for the analytical session. The dashed line is a best-fit line through data for the alkali-rich, Ca-poor Mascota andesite (MAS) and shows a SIMS calibration factor of 0.25. This is slightly higher than the calc-alkaline MHA with a factor of 0.24. The solid lines are best-fit lines through data for the Mt. Hood andesite measured in 1997 (97). Note that the fit for andesite data measured in 1996 (96) has a similar slope.

ε_{5200} and ε_{4500} are the extinction coefficients of those two bands (L/mol/cm^{-1}), d is the sample thickness (cm), and ρ is the sample density (following the Beer-Lambert law above, Stolper 1982; Newman et al. 1986).

The extinction coefficients (ε_{5200} and ε_{4500}) resulting from a linear least squares fit of the data, corrected for the density of a volatile-free glass (ρ_o = 2565 g/L), are similar to those determined or calculated by other authors (Table 4). Our fit gives ε_{4500} and ε_{5200} within error of each other, although most other authors find that $\varepsilon_{4500} < \varepsilon_{5200}$ (excepting data for phonolite and rhyolite in Table 4). The errors for our extinction coefficients are large due to poor quality 5200 cm^{-1} and 4500 cm^{-1} peaks that were observed at various sample thicknesses (Fig. 1a, Table 4). Because the peaks have large errors, the data do not produce statistically significant fits using an expanded Taylor polynomial approach (e.g., Zhang et al. 1997).

The 3550 cm^{-1} H_2O peak was assumed to represent H_2O_{total} (Dixon et al. 1995) and the extinction coefficient (ε_{3500}) was determined using the Beer-Lambert law (Fig. 4a, Table 4), corrected for ρ_o. Again, these values are similar to those determined by other authors for intermediate compositions (Table 4). For thick samples or those with high H_2O_{total} contents, the 3550 cm^{-1} peak is saturated and some authors have used the 3100 cm^{-1} shoulder to determine H_2O_{total} to within 10% (Danyushevsky et al. 1993). This technique is also valid for our samples (Fig. 4a, Table 4), indicating that within the compositional range the shape of the 3550 cm^{-1} peak does not vary greatly. The result that the 3100 cm^{-1} shoulder shows a better correlation with the total H_2O data than the 3550 cm^{-1} peak (Fig. 4a) could indicate difficulties with the "straight line" baseline subtraction method. The 1630 cm^{-1} peak was calibrated using H_2O_{mol} contents from the 5200 cm^{-1} peak (Fig. 4b) and is also within the range of expected values (Table 4).

C-O species. Since the CO_2 concentrations in our samples were low relative to the error for the manometry measurements it was not possible to reliably determine extinction coefficients for the C-O species. We note that Morizet et al. (2002) also found that the CO_3^{2-} extinction coefficient (ε_{1550}) was difficult to determine for haplo-phonolite glasses. Thus, we estimated a ε_{1550} of approximately 271 L/mol/cm^{-1} using the Na/(Na + Ca) content following Dixon and Pan (1995). We suggest that the error in their technique is likely less than about 10% based on ε_{1550} values that have been presented subsequently (Jakobsson 1997; Jendrzejewski et al. 1997). For the $CO_{2\,mol}$ extinction coefficient (ε_{2350}), we used the value for Na-Al-Si-O glasses (945 L/mol/cm^{-1}; Fine and Stolper 1985), which is within 16% of the values measured for rhyolite (1066 Lmol^{-1}cm^{-1}; Blank 1993) and haplo-phonolite (796 ± 250 L/mol/cm^{-1} synthesized at 1300 °C; Morizet et al. 2002). If these estimated extinction coefficients are applied to the data, the micro-FTIR $CO_{2\,total}$ contents

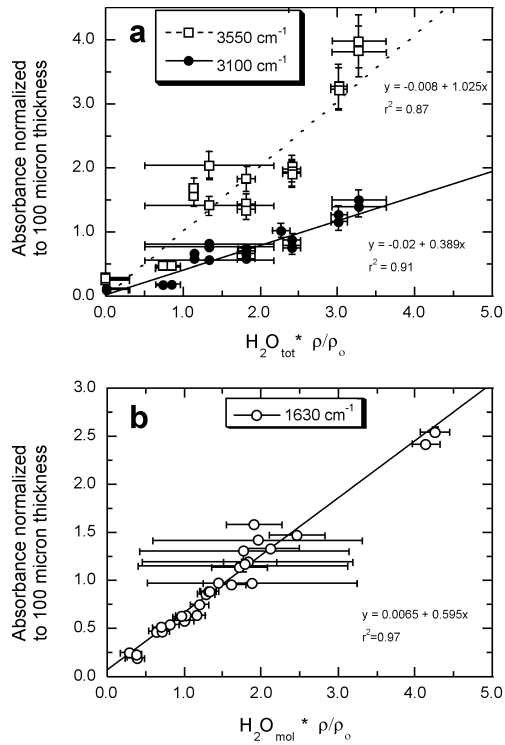

FIGURE 4. (**a**) 3550 cm^{-1} peak absorbances and 3100 cm^{-1} slope absorbances normalized to 100 mm vs. $\rho/\rho_0 \cdot H_2O_{total}$ (by SIMS or manometry). (**b**) 1630 cm^{-1} absorbances normalized to 100 mm vs. $\rho/\rho_0 \cdot H_2O_{mol}$ from the 5200 cm^{-1} absorbance. In both plots, ρ_0 is the density of the nominally volatile-free sample. The slope of the regression line for each peak is related to the extinction coefficient following: slope = $(\rho_0 \cdot e_{peak})$/(molecular weight of species$\cdot 10^4$). Error bars for H-O FTIR absorbances are based on the maximum and minimum peak baselines.

are within error of the values determined by incremental-heating manometry (Tables 2 and 3). However, the micro-FTIR $CO_{2\ total}$ contents are substantially lower than the values determined by bulk manometry, possibly because bulk techniques include C contributions from surface contamination or fluid inclusions.

Electron probe micro-analysis deficits

The measured H_2O_{total} contents by manometry and SIMS are reported along with the electron microprobe deficits, corrected for $CO_{2\ total}$ content in Table 2. For most samples, the different measurements agree within about 1 wt% (absolute) of the measured H_2O_{total} contents (similar to findings for andesites through high silica rhyolites; Devine et al. 1995). Samples Juli9 and MHA26 have electron probe deficits from different analytical sessions that are within error and these just exceed 1 wt% of the values determined by SIMS and manometry. Three samples (MHA12, MHA27, and MHA18) have electron probe deficits that are more than 1 wt% higher than the other measurements. Sample MHA18 was only measured in 2001, does not appear to have degassed, and the large discrepancy between the electron probe deficit and the other measurements is likely due to Na-"loss," which was difficult to avoid with this H_2O-rich sample (note the relatively low Na_2O content in Table 2). Samples MHA12 and MHA27 may have degassed during the time between the different measurements because electron probe deficits measured during 1996–1998 are higher than measurements made in 2001 (Table 2). The hypothesis that H_2O was lost over time is supported by evidence from FTIR (P.L. King, unpublished data). Furthermore, samples with highly depolymerized structures (e.g., peralkaline rocks) "lose" water at temperatures as low as 50 °C (Moore et al. 1998) and we suggest that samples with high H_2O contents, that are also highly depolymerized, may similarly have high water diffusion rates.

We suggest that the electron microprobe may be used to calculate H_2O content for most samples within about 1 wt% for samples with moderate H_2O contents, but analyses must be corrected for other volatiles (e.g., CO_2), care must be taken to avoid Na-"loss," Al- and Si-"grow in," and the degassing history of the samples must be known (similar to conclusions of Devine et al. 1995).

DISCUSSION

A model for SIMS H calibration factors in minerals and glasses

To determine the sensitivity of SIMS to measurements of H-content for a range of mineral and glass compositions, we compared the SIMS H calibration factors (SIMS Hcf) for MHA, MAS and a range of other compositions to factors related to the sample matrix, such as volatile-free molar weight, mean atomic number, atomic density, and compositional parameters (e.g., Na/(Na + Ca), Fe/Mg, non-bonding oxygens/tetrahedral oxygens etc.). This approach is similar to those developed to model relative sensitivity factors and used to determine factors for oxygen isotope instrumental mass fractionation (Hervig et al. 1992; Eiler et al. 1997). The glasses we examined (Fig. 5) have relatively constant compositions, with variations in the H content, excepting the basaltic glass suite where different basalt compositions were used (Ihinger et al. 1994) and the minerals, which also showed some variability. Since Fe^{3+}/Fe^{2+} was not known in most of the samples, we accounted for Fe^{3+}/Fe^{2+} variation by examining the extreme values (all Fe^{3+} or all Fe^{2+}).

The SIMS Hcf values show a reasonable correlation with molar weight (MW, g/mol) normalized to a one-oxygen mole of the volatile-free composition. Other methods of quantifying the matrix did not show a good correlation with SIMS Hcf. The negative correlation suggests that the H ion intensity per unit H abundance decreases with increasing molar weight of the target.

A linear regression to the data gives a relationship that allows for the determination of SIMS Hcf. The regression equation fits the homogeneous glass data well, while the more heterogeneous minerals and basalts tend to fall off the regression line, with phlogopite SIMS Hcf (Righter et al. 2002) lying outside the range of the remaining data. If the outlier phlogopite data is omitted, the regression equation is: SIMS Hcf = 1.393 – 0.03393·(MW), with $r^2 = 0.90$. If phlogopite is included, the regression equation is: SIMS Hcf = 1.319 – 0.03169·(MW), with $r^2 = 0.81$. The difference in fit does not significantly affect materials with molar weights between 32 and 36 g/mol, but for materials with MW close to 40 g/mol (e.g., humite minerals and micas), the equations predict SIMS Hcf that differ by

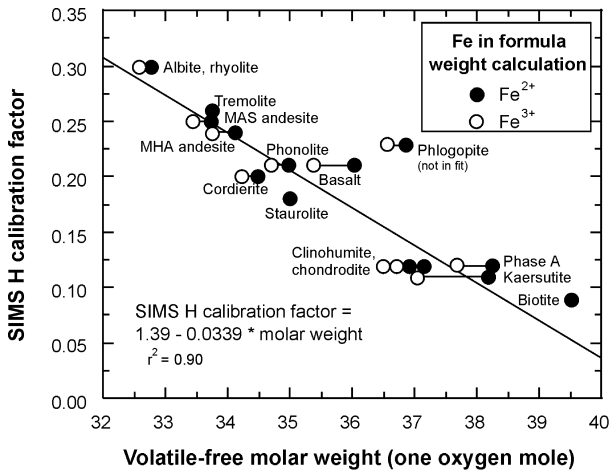

FIGURE 5. SIMS H calibration factors for a variety of compositions plotted vs. volatile-free molar weight (g/mol, based on a 1 oxygen mole). The variation in composition arises from the assumption that all Fe occurs as either Fe^{2+} or Fe^{3+} or from variations in the standards used. The data are from Ihinger et al. (1994), Kawamoto et al. (1994), King (1999), Righter et al. (2002), and unpublished data from the ASU SIMS laboratory. The fit to the data, excluding the outlier phlogopite, is: SIMS Hcf = 1.393 – 0.03393·(MW), with $r^2 = 0.90$. If phlogopite (Righter et al. 2002) is included, the fit equation is: SIMS Hcf = 1.319 – 0.03169·(MW), with $r^2 = 0.81$.

about 25%. Whereas both regressions show a high correlation, there is some scatter around the regression line that likely arises from: (1) normalizing the H^+ count rate to $^{30}Si^+$ because the trend could result from increasing $^{30}Si^+$ yields with increasing molar weight, (2) assuming that the chemistry of the bulk is identical to the chemistry of the surface during an analysis even though the $^{16}O^-$ beam is implanted in the surface, (3) problems with the bulk volatile analysis of the samples for calibration (e.g., Ihinger et al. 1994); and 4) assuming that the "volatile-free molar weight" represents the sample matrix when the actual samples used for calibration contain volatiles.

Despite the scatter, we suggest that the empirical relationship [SIMS Hcf = 1.393 – 0.03393·(MW)] will give H contents with a conservative error of 20% relative to the molar weight range of 32 and 36 g/mol. The data also indicate that a more precise calibration model might be gained from a systematic study of H yields in different matrices, monitoring variations in matrix chemistry and sputter yields (e.g., Eiler et al. 1997).

C-O-H speciation: controls on variation

Natural silicate glasses contain volatiles that are dominated by H-O species with subordinate C-O-S-N-Cl species (Carroll and Holloway 1994). The variations in H-O species in glasses are attributed to variation in the H-O species in melts with different H_2O_{total} contents and different quench rates (Withers et al. 1999; Nowack and Behrens 2001). We find that molecular H_2O and OH^- contents vary with increasing H_2O_{total} content in a manner similar to other studies and speciation model curves (models reviewed in Dixon et al. 1995).

Analogous with the H-O species, the variation in C-O speciation and CO_3^{2-} peak splitting in the glasses is considered to represent melt speciation. However, unlike the H-O species, our data show that CO_3^{2-} and $CO_{2\ mol}$ contents, in a given melt composition, vary as a function of both $CO_{2\ total}$ and H_2O_{total} (King and Holloway 2002). For all samples, as $CO_{2\ total}$ increases, there is no obvious trend in C-O species (Table 2). Molecular CO_2 and CO_3^{2-} contents are extremely low (<0.1 wt%) for the samples that did not initially have a C-source. For the samples with a C-source added, as H_2O_{total} increases, $CO_{2\ mol}$ decreases slightly and CO_3^{2-} increases slightly (Table 2). Also, as H_2O_{total} increases, the distance between CO_3^{2-} peaks decreases (Fig. 6). A decrease in CO_3^{2-} peak splitting was also observed in other compositions and corresponds to increasing degeneracy of the CO_3^{2-} bonding environment (Taylor 1990; Jakobsson 1997). These results differ from those on icelandite where, although the CO_3^{2-} splitting decreases with increasing H_2O_{total}, $CO_{2\ mol}$ was present only in the most H_2O_{total}-rich sample (Jakobsson 1997). We are uncertain why this discrepancy exists, but it could be due to different C dissolution mechanisms in icelandite.

Dissolution mechanisms for C in aluminosilicate glasses are reviewed by Blank and Brooker (1994). One suggestion is that the changes in C-O speciation are primarily related to different glass transition temperatures (Blank and Brooker 1994; Brooker et al. 1999). However, the dependence of the glass transition temperature on the H_2O_{total} content means that it is difficult to separate those two factors. Another probable reason is that $CO_3^{2-}/CO_{2\ mol}$ increases with increasing H_2O as the melt structure becomes less polymerized. This proposal is supported by changes in C-O speciation and carbonate peak splitting data as a function of composition (polymerization) (Brooker et al. 1999; Brooker et al. 2001). These trends are discussed in more detail in King and Holloway (2002).

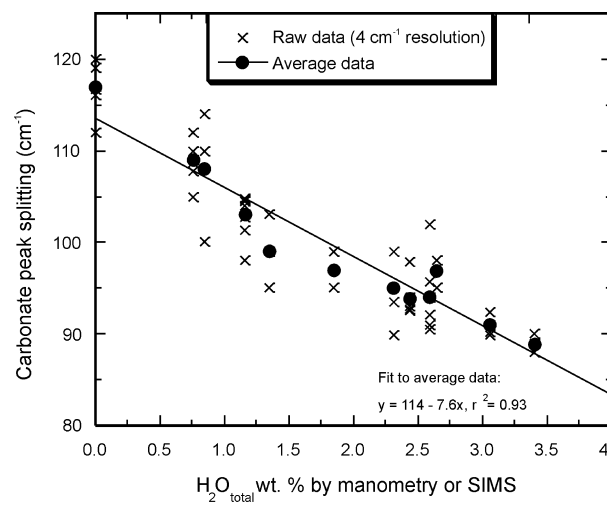

FIGURE 6. FTIR CO_3^{2-} peak splitting vs. and H_2O_{total} determined by manometry or SIMS. Note that the peak splitting decreases with increasing H_2O content, indicating increasing degeneracy of the CO_3^{2-} bonding environment.

Recommendations for micro-analysis of volatiles

Bulk manometry has the advantage of ease of sample preparation, but standard techniques require a relatively large volume of sample dependent on volatile concentration (10–100s of mg). The results of this study indicate that bulk manometry of glasses may overestimate C due to adsorption of volatiles and/or contamination by carbon-bearing species below the glass transition temperature. We recommend using incremental-heating manometry, perhaps in tandem with stable isotope analyses, to determine whether C contamination has occurred in high-pressure experiments.

SIMS analysis for H_2O content in glasses has the advantages of excellent spatial resolution (<200 μm^2) and precision, and can be used for both glasses and minerals. For highest confidence in the SIMS analyses, it is preferable to have standards similar in bulk chemistry to the unknowns. In the absence of these standards, the empirical equation presented here can be used. However, examination of Figure 5 shows that the equation may lead to systematic errors in the H analysis of phases with high molar weights, such as the humite minerals and micas. Until the SIMS calibrations for H are extended to such phases, the analyst may need to consider alternative techniques for the determination of H contents.

Micro-FTIR is calibrated for H-O species in several natural intermediate glasses (Table 4) and has the advantages of spatial resolution, but the disadvantage of tedious sample preparation for transmission analysis. The values for H-O species extinction coefficients in the C-O-H-bearing andesites agree with literature results, indicating that C-O species do not affect H-O calibrations. Our data was insufficient to determine C-O species extinction coefficients because $CO_{2\ total}$ concentrations were low relative to the error of manometric measurements and also because H_2O strongly affects C-O speciation. However, we found that estimates of the extinction coefficients for CO_3^{2-} and $CO_{2\ mol}$ likely have about 10 and 16% error, respectively. Calculation of $CO_{2\ total}$ contents based on these estimates compare well with $CO_{2\ total}$ from incremental-heating manometry.

Our data indicates that H_2O contents determined for andesitic glasses with known $CO_{2\ total}$ contents using electron microprobe deficits are accurate to within about 1 wt% absolute, relative to manometry and SIMS analyses for samples with moderate H_2O contents. Thus the electron probe is a viable method of determining H_2O contents of glasses, provided that care is taken to avoid Na-"loss," Al- and Si-"grow in," that all other volatile species are known, and the degassing history of the glass is known. We recommend that SIMS or micro-FTIR be used in preference to the electron probe for glasses with low H_2O contents (<1.5 wt%) or high H_2O contents (>3 wt%) and reiterate that the electron probe is inadequate for analysis of volatiles in oxy-substituted minerals (e.g., Dyar et al. 1993; King et al. 1999).

ACKNOWLEDGMENTS

We thank J. Gardner and J. Dixon for helpful reviews. E. Hauri is thanked for ^{12}C ion probe analysis and P. Middlestead for help with bulk C analysis of the Mt. Hood andesite starting material. D. Eggler provided the Mt. Hood andesite composition powder and G. Moore provided Mascota andesite (MAS) glass samples. The following people are thanked for helpful discussions: G. Moore, S. Jakobsson, D. Vielzeuf, H.D. Zimmerman, A. Grzechnik, L. Danyushevsky, and K. Roggensack. M. Carroll and S. Newman provided computer programs for the density calculations. The USGS Menlo Park provided access to their micro-FTIR. This work was supported by NSF grants EAR-9506494 (Holloway), EAR-9614325 (Hervig and Holloway) and EAR-9614229 (McMillan) and by an NSERC operating grant (King).

REFERENCES CITED

Agrinier, P. and Jendrzejewski, N. (2000) Overcoming problems of density and thickness measurements in FTIR volatile determinations: a spectroscopic approach. Contributions to Mineralogy and Petrology, 139, 265–272.

Blank, J.G. (1993) An experimental investigation of the behavior of carbon dioxide in rhyolitic melt. Ph.D. dissertation, California Institute of Technology, Pasadena, CA.

Blank, J.G. and Brooker, R.A. (1994) Experimental studies of carbon dioxide in silicate melts: Solubility, speciation, and stable carbon isotope behavior. In M.R. Carroll and J.R. Holloway, Eds., Volatiles in Magmas, 30, p. 157–186. Reviews in Mineralogy, Mineralogical Society of America, Washington, D.C.

Brearley, M. and Montana, A. (1989) The effect of CO_2 on the viscosity of silicate liquids at high pressure. Geochemica et Cosmochimica Acta, 53, 2609–2616.

Brooker, R., Holloway, J.R., and Hervig, R. (1998) Reduction in piston-cylinder experiments: The detection of carbon infiltration into platinum capsules. American Mineralogist, 83, 985–994.

Brooker, R.A., Kohn, S.C., Holloway, J.R., McMillan, P.F., and Carroll, M.R. (1999) Solubility, speciation and dissolution mechanisms of CO_2 in melts along the $NaAlO_2$-SiO_2 join. Geochemica et Cosmochimica Acta, 63, 3549–3565.

Brooker, R.A., Kohn, S.C., Holloway, J.R., and McMillan, P.F. (2001) Structural controls on the solubility of CO_2 in silicate melts. Part II: IR characteristics of carbonate groups in silicate glasses. Chemical Geology, 174, 241–254.

Carroll, M.R. and Blank, J.G. (1997) The solubility of H_2O in phonolitic melts. American Mineralogist, 82, 549–556.

Carroll, M.R. and Holloway, J.R. (1994) Volatiles in Magmas. Reviews in Mineralogy, 30, p. 517. Mineralogical Society of America, Washington, D.C.

Danyushevsky, L.V., Falloon, T.J., Sobolev, A.V., Crawford, A.J., Carroll, M., and Price, R.C. (1993) The H_2O content of basalt glasses from southwest Pacific back-arc basins. Earth and Planetary Science Letters, 117, 347–362.

Delaney, J.R. and Karsten, J.L. (1981) Ion microprobe studies of water in silicate melts: Concentration-dependent water diffusion in obsidian. Earth and Planetary Science Letters, 52, 191–202.

Des Marais, D.J. (1986) Carbon abundance measurements in oceanic basalts: the need for consensus. Earth and Planetary Science Letters, 79, 21–26.

Des Marais, D.J. and Moore, J.G. (1984) Carbon and its isotopes in mid-oceanic basaltic glasses. Earth and Planetary Science Letters, 69, 43–57.

Devine, J.D., Gardner, J.E., Brach, H.P., Layne, G.D., and Rutherford, M.J. (1995) Comparison of microanalytical methods for estimation of H_2O contents of silicic volcanic glasses. American Mineralogist, 80, 319–328.

Dingwell, D.B. and Webb, S.L. (1990) Relaxation in silicate melts. European Journal of Mineralogy, 2, 427–449.

Dixon, J.E. and Pan, V. (1995) Determination of the molar absorptivity of dissolved carbonate in basanitic glass. American Mineralogist, 80, 1339–1342.

Dixon, J.E., Stolper, E.M., and Holloway, J.R. (1995) An experimental study of water and carbon dioxide solubilities in mid-ocean ridge basaltic liquids. Part I: Calibration and solubility models. Journal of Petrology, 36, 1607–1631.

Dyar, M.D., Guidotti, C.V., Holdaway, M.G., and Colucci, M. (1993) Nonstoichiometric hydrogen contents in common rock-forming hydroxyl silicates. Geochimica et Cosmochimica Acta, 57, 2913–2918.

Eggler, D.H. and Burnham, C.W. (1973) Crystallization and fractionation trends in the system andesite-H_2O-CO_2-O_2 at pressures to 10 kb. Geological Society America Bulletin, 84, 2517–2532.

Eiler, J.M., Graham, C., and Valley, J.W. (1997) SIMS analysis of oxygen isotopes: matrix effects in complex mineral and glasses. Chemical Geology, 138, 221–244.

Fine, G.J. and Stolper, E.M. (1985) The speciation of carbon dioxide in sodium aluminosilicate glasses. Contributions to Mineralogy and Petrology, 91, 105–121.

Hauri, E., Wang, J., Dixon, J.E., King, P.L., Mandeville, C., and Newman, S. (2002) SIMS analyses of volatiles in volcanic glasses. 1: Calibration, matrix effects and comparisons with FTIR. Chemical Geology, 183, 99–114.

Hervig, R.L., Williams, P., Thomas, R.M., Schauer, S.N., and Steele, I.M. (1992) Microanalysis of oxygen isotopes in insulators by secondary ion mass spectrometry. International Journal of Mass Spectrometry and Ion Processes, 120, 45–63.

Holloway, J.R., Burnham, C.W., and Millhollen, G.L. (1968) Generation of H_2O-CO_2 mixtures for use in hydrothermal experimentation. Journal of Geophysical Research, 73, 6598–6600.

Ihinger, P.D., Hervig, R.L., and McMillan, P.F. (1994) Analytical methods for volatiles in glasses. In M.R. Carroll and J.R. Holloway, Eds., Reviews in Mineralogy, 30, p. 67–121. Mineralogical Society of America, Washington, D.C.

Jakobsson, S. (1997) Solubility of water and carbon dioxide in an icelandite at 1400°C

and 10 kilobars. Contributions to Mineralogy and Petrology, 127, 129–135.
Jendrzejewski, N., Trull, T.W., Pineau, F., and Javoy, M. (1997) Carbon solubility in Mid-Ocean Ridge basaltic melt at low pressures (250-1950 bar). Chemical Geology, 138, 81–92.
Kawamoto, T., Leinenweber, K., Hervig, R.L., and Holloway, J.R. (1994) Stability of hydrous minerals in H_2O-saturated KLB-1 peridotite up to 15 GPa. In K.A. Farley, Ed., Volatiles in the Earth and Solar System. American Institute of Physics Conference Proceedings, 341, p. 229–239. AIP Press, Pasadena, CA.
King, P.L. (1999) C-O-H Volatiles in Igneous Rocks: Experimental and Natural Studies of Hydrous Minerals (Amphiboles) and Glasses (Melts). Ph.D. dissertation, Arizona State University, Tempe, AZ.
King, P.L. and Holloway, J.R. (2002) CO_2 solubility in intermediate (andesitic) melts. Geochimica et Cosmochimica Acta, 66, 1627–1640
King, P.L., Hervig, R.L., Holloway, J.R., Vennemann, T., and Righter, K. (1999) Oxy-substitution and dehydrogenation in mantle-derived amphiboles. Geochimica et Cosmochimica Acta, 63, 3635–3651.
Kohn, S.C. and Brooker, R.A. (1994) The effect of water on the solubility and speciation of CO_2 in aluminosilicate glasses along the join SiO_2-$NaAlO_2$. Mineralogical Magazine, 58A, 489–490.
Lange, R.A. and Carmichael, I.S.E. (1987) Densities of Na_2O-K_2O-CaO-MgO-FeO-Fe_2O_3-Al_2O_3-TiO_2-SiO_2 liquids: New measurements and derived partial molar properties. Geochimica et Cosmochimica Acta, 51, 2931–2946.
Macpherson C.G., Hilton D.R., Newman S., and Mattey D.P. (1999) CO_2, $^{13}C/^{12}C$ and H_2O variability in natural basaltic glasses: A study comparing stepped heating and FTIR spectroscopic techniques. Geochimica et Cosmochimica Acta, 63, 1805–1813.
Mandeville, C.W., Webster, J.D., Rutherford, M.J., Taylor, B.E., Timbal, A., and Faure, K. (2002) Determination of extinction coefficients for infrared absorption bands of H_2O in andesitic glasses. American Mineralogist, 87, 813–821.
Moore, G., Vennemann, T., and Carmichael, I.S.E. (1995) Solubility of water in magmas to 2 kbar. Geology, 23, 1099–1102.
——— (1998) An empirical model for the solubility of H_2O in magmas to 3 kilobars. American Mineralogist, 83, 36–42.
Morgan, G.B.V. and London, D. (1996) Optimizing the electron microprobe analysis of hydrous alkali aluminosilicate glasses. American Mineralogist, 81, 1176–1185.
Morizet, Y., Brooker, R.A., and Kohn, S.C. (2002) CO_2 in haplo-phonolite melt: solubility, speciation and carbonate complexation. Geochimica et Cosmochimica Acta, 66, 1809–1820.
Mysen, B.O. (1976) The role of volatiles in silicate melts: Solubility of carbon dioxide and water in feldspar, pyroxene, and feldspathoid melts to 30 kb and 1625°C. American Journal of Science, 276, 969–996.
Newman, S., Stolper, E.M., and Epstein, S. (1986) Measurement of water in rhyolitic glasses: calibration of an infrared spectroscopic technique. American Mineralogist, 71, 1527–1541.
Nowack, M. and Behrens, H. (2001) Water in rhyolitic magmas: getting a grip on a slippery problem. Earth and Planetary Science Letters, 184, 515–522.
Ohlhorst, S., Behrens, H., and Holtz, F. (2001) Compositional dependence of molar absorptivities of near-infrared OH^- and H_2O bands in rhyolitic to basaltic glasses. Chemical Geology, 174, 5–20.
Oskarsson, N., Sigvaldason, G.E., and Steinthorsson, S. (1982) A dynamic model of rift-zone petrogenesis and the regional petrology of Iceland. Journal of Petrology, 23, 28–74.
Ottolini, L., Bottazzi, P., and Zanetti, A. (1995) Determination of hydrogen in silicates by secondary ion mass spectrometry. Analyst, 120, 1309–1313.
Righter K., Dyar M.D., Delaney J.S., Vennemann T.W., Hervig R.L., and King P.L. (2002) Distribution of OH^-, O^{2-}, Cl^- and F^- in biotite from volcanic rocks and correlations with octahedral cations. American Mineralogist, 87, 142–153.
Shimizu, N. (1986) Silicon-induced enhancement in secondary ion emission from silicates. International Journal of Mass Spectrometry and Ion Processes, 69, 325–338.
Silver, L.A. (1988) Water in Silicate Glasses. Dept. Geological Planetary Sciences, Ph.D. dissertation, California Institute of Technology, Pasadena.
Steele, I.M. (1986) Ion probe determination of hydrogen in geologic samples. Neues Jahrhrub für Mineralogie Monatshefte, 1986, 193–202.
Stolper, E.M. (1982) Water in silicate glasses: an infrared spectroscopic study. Contributions to Mineralogy and Petrology, 81, 1–17.
Stolper, E., Fine, G., Johnson, T., and Newman, S. (1987) Solubility of carbon dioxide in albitic melt. American Mineralogist, 72, 1071–1085.
Taylor, W.R. (1990) The dissolution mechanism of CO_2 in aluminosilicate melts: Infrared spectroscopic constraints on the cationic environment of dissolved $[CO_3]^{2-}$. European Journal of Mineralogy, 2, 547–563.
Vennemann, T.W. and O'Neil, J.R. (1993) A simple and inexpensive method of hydrogen isotope and water analyses of minerals and rocks based on zinc reagent. Chemical Geology, 103, 227–234.
Wilson, R.G., Stevie, F.A., and Magee, C.W. (1989) Secondary Ion Mass Spectrometry: A Practical Handbook for Depth Profiling and Bulk Impurity Analysis. J. Wiley, New York.
Withers, A.C., Zhang, Y.X., and Behrens, H. (1999) Reconciliation of experimental results on H_2O speciation in rhyolitic glass using in-situ and quenching techniques. Earth and Planetary Science Letters, 173, 343–349.
Yamashita, S., Kitamura, T., and Kusakabe, M. (1997) Infrared spectroscopy of hydrous glasses of arc magma compositions. Geochemical Journal, 31, 169–174.
Zhang Y., Stolper E.M., and Wasserburg G.J. (1991) Diffusion of water in rhyolitic glasses. Geochimica et Cosmochimica Acta, 55, 441–456.
Zhang, Y., Belcher, R., Ihinger, P.D., Wang, L., Xu, Z., and Newman, S. (1997) New calibration of infrared measurement of dissolved water in rhyolitic glasses. Geochimica et Cosmochimica Acta, 61, 3089–3100.

MANUSCRIPT RECEIVED AUGUST 17, 2001
MANUSCRIPT ACCEPTED APRIL 25, 2002
MANUSCRIPT HANDLED BY WENDY BOHRSON